sciendo

Polish Journal of Chemical Technology, 26, 4, 72—80, 10.2478/pjct-2024-0042

Optical shadowgraphy analysis of gas bubble equivalent diameters: Factors influencing measurement accuracy in bubble flows

Przemysław A. Luty*, Mateusz R. Prończuk, Katarzyna D. Bizon

Faculty of Chemical Engineering and Technology, Cracow University of Technology, Warszawska 24, Kraków 31-155, Poland

**Corresponding author: e-mail:* przemyslaw.luty@doktorant.pk.edu.pl

The article explores the impact of various factors on the determination of gas bubble equivalent diameters using optical shadowgraphy. The experimental setup involves a liquid-gas system. The results indicate that the distance between the camera and the bubble rise-up plane has negligible influence on measurement precision as long as the area captured is constant. Increasing the number of analyzed frames significantly reduces uncertainties, while higher image magnification leads to increased uncertainties due to a reduced number of frames and smaller area captured. Image distortion correction minimally affects results and precision. The study concludes that factors such as resolution, frame rate, and elongated flow path captured contribute to more accurate determination of equivalent bubble diameters, essential for the determination of mass and heat transfer coefficients in liquid-gas flows. The results indicate that a sufficiently high number of video frames may be more important than indiscriminately increasing the resolution.

Keywords: shadowgraphy, optical imaging, bubbling, bubble diameter, bubble flow, image distortion.

INTRODUCTION

Multiphase flow encompasses various modalities and configurations of phases, including the two-phase liquid-gas flow. This type of flow involves a liquid phase as the continuous medium, while the gas phase is usually in the form of dispersed bubbles that flow through the liquid layer. The process of bubbling, which consists of the simultaneous movement of numerous gas bubbles within a liquid, is of great importance in several sectors of modern industry, including chemical, petrochemical, and biochemical industries[1–3].

Bubbling offers several key advantages, including efficient liquid mixing facilitated by the movement of gas bubbles, which often eliminates the need to employ mechanical stirrers. Additionally, it provides a well-developed interface between the liquid phase and the gas phase, leading to high mass and heat transfer coefficients between the two phases[4, 5]. To take full advantage of the bubbling benefits, it is crucial to understand the hydrodynamic characteristics of gas bubbles as they rise through the liquid layer. This involves determining parameters such as the number of bubbles per unit volume, their size and shape, and flow velocity[6]. Kulkarni and Joshi[7] extensively reviewed the most significant theoretical and empirical models for evaluating these hydrodynamic parameters of gas bubbles.

The hydrodynamic characteristics of gas bubbles can be determined using various multidimensional measurement techniques, including optical techniques. Optical techniques, such as particle image velocimetry[8] and shadowgraphy[9], play nowadays a significant role in this regard.

In particle image velocimetry (PIV), very fine solid particles acting as a tracer are added to the fluid and illuminated by a laser. Next, images of the gas bubbles flowing through a liquid containing solid particles are captured and analyzed. Based on the changes of the location and orientation of the particles it is possible to determine system parameters, such as fluid velocity field around the gas bubble[10]. Due to the presence of seeding particles that may influence the velocity field, PIV generally is an invasive measurement method. However, its invasiveness is low, hence it is often classified as non-intrusive technique[8, 10, 11]. Generally, PIV is used in various areas, such as two-phase flow through pipes, aerodynamics, turbulence research or combustion[10]. When considering liquid-gas flows, PIV can be used to investigate flow structures and patterns in flows of high void fraction, such as slug flow[8, 12].

In shadowgraphy, images are captured exclusively using an external light source with no need for any form of direct invasion into the system[13, 14]. Therefore, a major advantage of shadowgraphy is its totally non-invasive character[15]. Shadowgraphy is used widely to investigate flow structures in two-phase bubbly flows[16]. However, it can be employed also for the analysis of two-phase gas-liquid system, in which gas is a continuous phase. For instance, Emberson et al.[17] investigated Diesel and Diesel-water emulsion spray injection using shadowgraphy. Considering bubbly flows, when light passes through the liquid-gas interface surrounding a gas bubble, it is refracted, which results in a visible dark rim in the recorded images. By analyzing the location and shape of this dark rim, it is possible to determine the position and size of the bubble. Since the shape and velocity of the bubble fluctuate during the flow, and the recorded images represent a two-dimensional projection of the three-dimensional bubble, multiple images of the same bubble at different times during its flow need to be analyzed. By averaging the hydrodynamic properties of the bubble, such as equivalent diameter or deformation index, representative values can be obtained. Analyzing multiple images of the flowing bubble also enables the determination of its trajectory and flow velocity.

Other important non-invasive methods for the investigation of liquid-gas flows include phase Doppler anemometry (PDA)[18] and interferometric particle imaging (IPI)[19]. Ultrasonic tomography (UT)[20, 21], capillary suction probes (CSP)[19], conductivity probes[22] and wire-mesh sensors (WMS)[20, 23], are, in turn, invasive methods used to bubble research.

Reducing uncertainty when determining the equivalent diameter of a gas bubble through shadowgraphy can be achieved by increasing the number of analyzed images and improving their resolution. However, in cases when the camera is static, increasing the number of analyzed images may result in larger equivalent diameter values. This may be due to the following factors: the positioning of the camera not being perpendicular to the direction of bubble flow, loss of focus in the off-center location of the bubble (if the camera is focused on the image center), and image distortion caused by imperfections in the optical system, particularly the lens. The effect of changing the distance between the camera and the analyzed bubble is not straightforward either. While reducing the distance improves the resolution of the recorded image and thus of the bubble, it also limits the maximum number of images that can be analyzed for a given bubble.

Despite the widespread use of shadowgraphy in studying bubble flows, there is currently no complex analysis of the impact of camera parameters, camera-to-bubble distance, and the number of analyzed images on the uncertainty associated with determining the equivalent diameter of gas bubbles reported in the scientific literature.

This study aims to experimentally verify the effects of various factors, including the distance between the averaged bubble rise-up plane and the outer lens of the camera, image magnification (zoom) related to bubble image resolution, the number of analyzed video frames per bubble, and image distortion correction, on the values of gas bubble equivalent diameters and their associated uncertainties determined using the optical shadowgraphy method.

MATERIALS AND METHODS

Experimental setup

Figure 1 illustrates the experimental setup used in this study. The constructed stand was straightforward. Tap water was used as the liquid phase, while air was used as the gas phase. The experiments were conducted at an ambient temperature of approximately 21 °C. Gas flow was achieved through compressor-generated overpressure (indicated with number 1 in Fig. 1), and was controlled using a valve (located under the liquid tank, not visible in Fig. 1). The gas was introduced into the lower section of the liquid tank (number 4 in Fig. 1) via a brass nozzle (number 2 in Fig. 1). To achieve bubbles characterized by different equivalent diameters, four different nozzles with internal diameters of 0.8 mm, 1.5 mm, 2.0 mm, and 3.0 mm were utilized in the experiments. The liquid tank, constructed from acrylic glass, had a rectangular cross-section with side lengths of 27 cm and 17 cm. The tank was filled with stagnant liquid up to a height of 55 cm, and the gas distributor nozzle was partially submerged in the liquid, with its outlet directed vertically upward. The gas flowed through the liquid layer in the form of bubbles, with the analyzed bubble flow path that was approximately 6.5 cm or 15 cm, depending on the experimental case. The center of the bubble flow path was located at the height of the camera, i.e. 24 cm above the bottom of the liquid tank. To ensure high-quality video recordings of the bubble flow, a LED backlight was positioned behind the liquid tank (number 5 in Fig. 1). Videos were captured using an AOS Promon U1000 monochrome camera (number 3 in Fig. 1) capable of recording grayscale video at a maximum resolution of 1984 × 1264 pixels at frame rate 139 frames per second (fps). It allows to increase frame rate when recording at a lower resolution. The camera was equipped with Kowa LMZ69M lens with a variable focal length of 11.5-69 mm and connected to a computer. The frame rate was set to 300 frames per second (fps) for the experiments. The recorded videos had resolutions of either 1984 × 500 pixels or 1984 × 564 pixels, depending on the distance between the averaged plane of bubble rise-up and the camera.

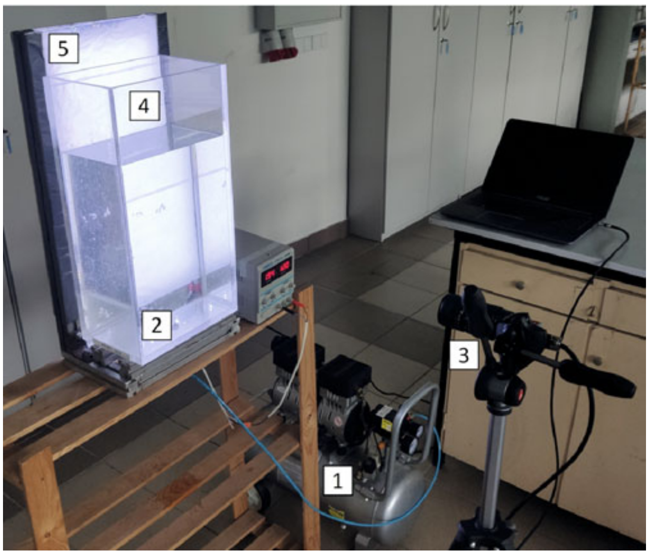

Figure 1. Photograph of the experimental setup: 1 – compressor, 2 – brass nozzle, 3 – high-speed camera, 4 – liquid tank, 5 – LED backlight

Experimental procedure

The experiments performed within this study consisted of capturing videos showing the flow of gas bubbles through a stagnant liquid layer. To achieve a nearly static bubble formation mechanism, the gas flow rate was controlled using a valve set at a low level. Each recorded video frame contained only one visible bubble. Image processing techniques were employed to analyze the recorded videos and to determine the size of the rising gas bubbles. The specific procedure is described in detail further in this subsection.

A non-invasive shadowgraphy method was utilized to determine the equivalent diameters of the gas bubbles[23]. In the recorded images, the LED backlight positioned behind the liquid tank caused light refraction at the liquid-gas interface, resulting in a dark rim surrounding the gas bubble. The geometric parameters of each bubble were computed based on the size and shape of this rim by using built-in Matlab functions as described more comprehensively in subsection 2.3.

Since the shape of each analyzed gas bubble changed during its flow (Fig. 2), the calculated equivalent diameters varied across different video frames. According to Wichterle et al.[24], the bubble oscillation frequency for the water-air system for a range of bubble diameters of 3–9 mm is about 5–7 Hz, which coincides with observations from the research described in this article. Similar oscillation frequencies are reported for other systems studied by Wichterle et al.[24]. Nowadays, almost every camera allows video recording at the frame rate of at least 30 fps as a standard (often it is even 60 fps or higher). This is 4–6 times faster than the expected frequency of bubble oscillations. Nevertheless, in this work, a frequency of 300 fps was used so that the results of the experiments reflect very accurately the changes in the shape of the rising gas bubbles without privileging periodically repeating shapes, which could generate systematic errors. A Matlab script was developed to analyze the recorded videos frame-by-frame in an automatic manner. The equivalent diameter of a bubble was ultimately determined by calculating the arithmetic mean of the equivalent diameters obtained from 14 to 79 video frames, depending on the specific case, for the flow of the corresponding bubble in the liquid.

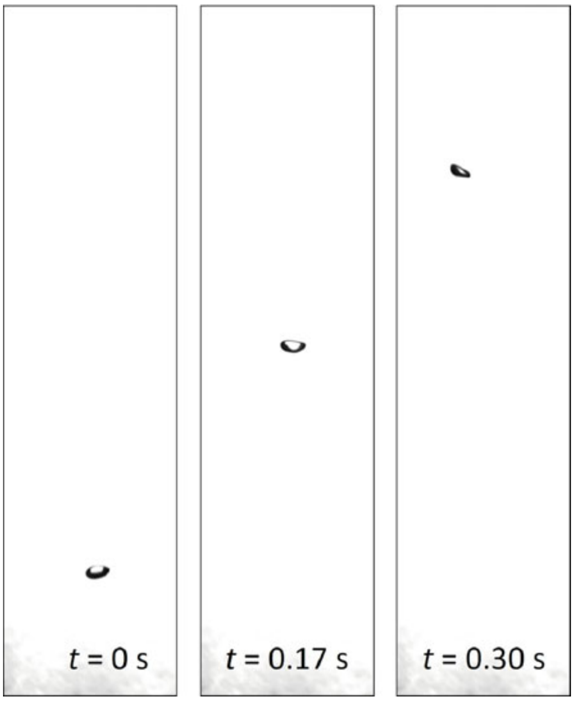

Figure 2. Visualisation of the shape change of a flowing gas bubble with an equivalent diameter of 3.24 mm

One of the objectives of the study was to examine the impact of the distance between the averaged plane of bubble rise-up and the camera on the uncertainty associated with determining the equivalent diameter of a gas bubble. Consequently, videos capturing the gas bubble flow were recorded from five different distances between the camera and the liquid tank.

Calculation procedure

The calculation procedure followed the methodology outlined in the previous work[23]. As presented in the mentioned work, this procedure gives results of bubble equivalent diameters very close to real values and is not sensitive to changes in image illumination.

All calculations were performed using Matlab 2021b software. The initial step involved detecting the rim surrounding the gas bubble in the analyzed monochromatic image (Fig. 3a). For this purpose, the Canny edge detector[25] was employed (Fig. 3b). The Canny edge detector operates by identifying local maxima of the gradient in the image, which has been pre-smoothed using a first-derivative Gaussian filter. Since the Canny edge detector works by searching for the maximum brightness gradient in an image, it is virtually unaffected by image brightness, which can be a concern with methods based on image brightness alone. Because of the total internal reflection of light on the outer edge of the gas bubble (the angle of incidence of light rays is close to 180°), the outer edge of the bubble shadowgraph is always the darkest spot in the image. Increasing the brightness of the illumination can brighten the inner edge of the bubble shadowgraph, but the outer edge remains virtually unchanged for a wide range of brightness settings. Thus, edge detection methods based on image brightness gradients can be considered reliable.

Subsequently, the region enclosed by the previously detected rim was filled, resulting in a binary black and white image (Fig. 3c).

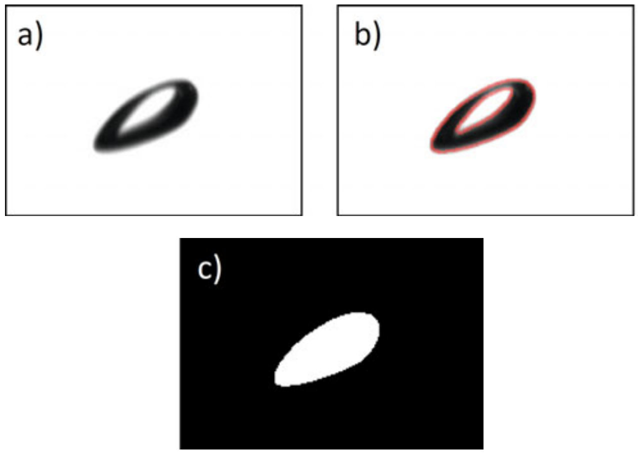

Figure 3. Subsequent stages of gas bubble detection in the image: a) unprocessed image, b) detected bubble rim, c) binary image after filling the interior of the detected rim

An additional issue investigated in this study was the application of image distortion correction, which influenced the obtained values of equivalent bubble diameters and their uncertainties. Due to imperfections in the optical system, particularly the lens used in the camera experiments, the recorded images exhibited a pincushion (i.e. positive) distortion. This distortion resulted in an increase in the size of objects captured in the images, with greater effect as the objects were positioned farther from the image center. To perform image correction, a set of calibration images was captured prior to each experimental series. These images consisted of photographs of a checkerboard pattern positioned perpendicular to the lens of the camera at a distance corresponding to the distance between the averaged bubble rise-up plane and the lens of the camera. An example of the effect of image distortion correction is presented in Fig. 4. Based on the calibration images, a set of parameters was obtained and subsequently utilized to correct the distortion in the images representing gas bubbles. The equivalent diameters of each analyzed gas bubble were calculated twice - once without applying image distortion correction and once with its application.

The processed image, following the aforementioned procedure, was then subjected to the Matlab *regionprops* function, which permits to compute the geometric parameters of the detected bubble, namely the maximum

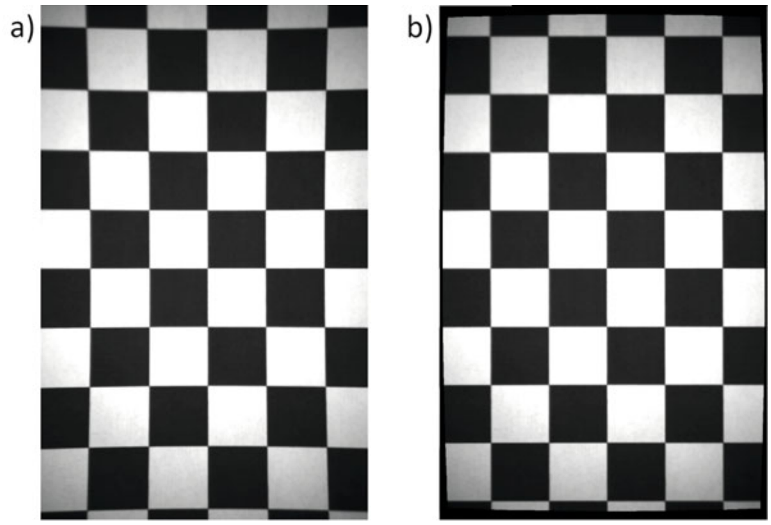

Figure 4. Image distortion correction: a) unprocessed calibration image, b) corrected calibration image

and minimum Feret diameters. The Feret diameter is a measure of particle elongation and is defined as the distance between two parallel lines tangential to the analyzed shape on opposite sides.

In the next step, the volume of a rotational ellipsoid representing the gas bubble was determined based on the maximum and the minimum values of the bubble Feret diameter for the given image. The Feret diameters were treated as the axes of the oblate rotational ellipsoid (spheroid), approximating the volume of the gas bubble to the volume of the ellipsoid calculated using the geometric parameters of the bubble projection on the plane. The volume of the rotational ellipsoid representing the gas bubble is expressed by the formula:

$$V_b = \frac{4}{3}\pi \frac{D_{F,max}^2 D_{F,min}}{8} C_{mp}^3 \quad (1)$$

where: V_b – calculated volume of the gas bubble [mm^3]; $D_{F,max}$ – maximum Feret diameter of the bubble projection [mm]; $D_{F,min}$ – minimum Feret diameter of the bubble projection [mm]; C_{mp} – conversion factor from pixels to millimeters [mm/pixel].

Conversion factor, C_{mp}, was determined using a sheet of millimeter paper placed in the plane of gas bubble rise. At the beginning of each series of experiments, a photo of a sheet of millimeter paper was taken, which later served as a length reference. The length conversion from pixels to millimeters was determined by reading the actual length in the image using a scale and dividing it by the distance in the image expressed in pixels. Subsequent videos were recorded without changing the position and settings of the camera. Thus, the length conversion factor could be used to estimate the size of the bubbles for the entire measurement series. The resulting conversion factor varied slightly depending on the measurement series and was equal to about 70 μm/pixel.

Finally, the equivalent diameter of the gas bubble was calculated as the diameter of a sphere with a volume equal to the previously calculated ellipsoid volume:

$$d_b = \sqrt[3]{\frac{6V_b}{\pi}} \quad (2)$$

where: d_b – calculated gas bubble equivalent diameter [mm].

Because of the change in hydrostatic pressure, the volume of the bubble changes with its distance from the surface of the liquid, and therefore the diameter of the bubble also changes. However, the pressure change caused by an additional 15 cm of water column (analyzed bubble flow path length) causes only a slight change in the diameter of the bubble. For a gas bubble with a diameter of 5 mm, the pressure change induced by a 15 cm water column causes a change in the diameter of the bubble of about 25 μm, which is much less than the resolution of the measurements made (70 μm/pixel). Therefore, it can be concluded that under the measurement conditions, the effect of hydrostatic pressure was negligibly small.

The uncertainties of the calculated gas bubble parameters were estimated using the standard deviations of the mean at a confidence level corresponding to ± 3σ. The uncertainties were propagated using the total differential method, which can be expressed by the general formula:

$$\delta f(x_1,\dots,x_n) = \sqrt{\left[\frac{\partial f(x_1,\dots,x_n)}{\partial x_1}\cdot\delta x_1\right]^2 + \dots + \left[\frac{\partial f(x_1,\dots,x_n)}{\partial x_n}\cdot\delta x_n\right]^2} \quad (3)$$

where: x_1, ..., x_n – arbitrary variables; $f(x_1, ..., x_n)$ – function of variables x_1, ..., x_n; δ – uncertainty in determining the value of the function or variable.

RESULTS AND DISCUSSION

In the first step, the influence of three factors on the values of equivalent diameters of gas bubbles and their uncertainties was examined:

– the distance between the averaged plane of bubble rise-up and the lens of the camera, x, using an approximation that ensures a constant area visible in the recorded images regardless of the distance,

– the number of analyzed frames, n, of a particular bubble flow,

– the application of distortion correction on the recorded images.

The distances between the averaged plane of bubble rise-up and the lens of the camera employed in the experiments were, respectively, 52.5 cm, 69 cm, 85.5 cm, 102 cm and 118.5 cm. The limit values were due to hardware limitations related to the camera lens parameters. It was not possible to position the camera closer than 52.5 cm due to the inability to focus the image properly. Similarly, it was not possible to move the camera further than 118.5 cm, as it would result in the inability to achieve the desired image magnification (zoom). Below, the outcome of the analysis performed on the fragments of videos consisting of 42 and 20 frames, respectively, depending on the considered case is reported. For each nozzle, four bubbles were generated, and then the average values of equivalent bubble diameters along with their uncertainties were calculated for each nozzle. The results are presented in Fig 5. The bubble rise-up velocity ranged from approximately 0.2 to 0.3 m/s and was practically independent of the bubble equivalent diameter.

As can be seen in Fig. 5, the results obtained indicate that the change in distance between the averaged plane of bubble rise-up and the camera, using magnification that ensures a constant area visible in the recorded images regardless of the distance, had a negligible effect on the obtained diameters. This is due to the similar resolution of the recorded images of the bubbles and the number of analyzed frames for each bubble, which was consistent across all cases.

The situation is different when it comes to decreasing the number of analyzed frames concerning the flow of a particular gas bubble, which is related to the length of the analyzed bubble flow path. The comparison of results obtained for different numbers of video frames taken to calculate bubble diameters is visible in Fig. 5. By individually considering the obtained values of the equivalent diameter for each frame concerning the flow of a specific bubble and assuming that the shape of the bubble remains unchanged during its flow, it can be concluded that these results best reflect the actual size of the bubble for the frame where the bubble is centrally positioned in front of the camera, i.e., the frame where the bubble is in its center. Each frame of a given video contains a certain error resulting from the projection of three-dimensional objects, such as gas bubbles, onto a plane (which is a two-dimensional object), with a larger error occurring the farther the bubble is located from the image center. The frames where the bubble is centrally positioned in front of the camera also have an error, but it is negligible. Several factors contribute

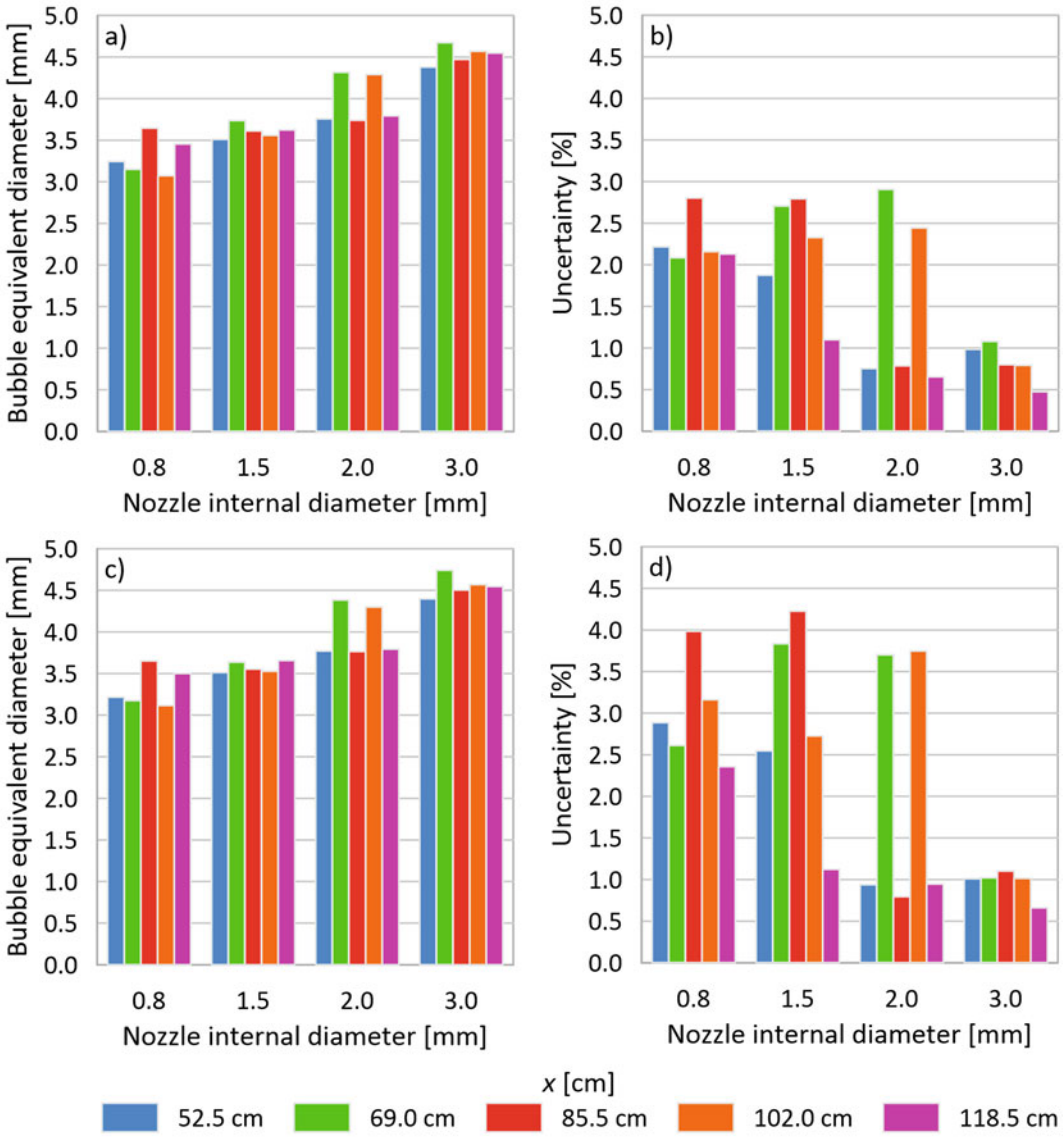

Figure 5. Bubble equivalent diameters (on the left) and their relative uncertainties (on the right) obtained from 42 video frames (a, b) and 20 video frames (c, d), no distortion correction applied.

to this error. Firstly, the farther from the image center bubble is positioned, the lower the sharpness of the projection of the visible bubble is (assuming the focus is set at the image center, as in this work). This effect is shown in Fig. 6. Secondly, the farther from the image center bubble is, the more elongated the projection of the bubble becomes in the recorded image due to the actual distance of the bubble from the camera lens. The bubbles are usually flattened, so if the camera is positioned perpendicular to the axis of their rise-up, the bubbles are at a certain angle in the upper and lower parts of the frame, which can cause the bubbles to appear elongated. This effect increases as the camera distance from the object decreases. For small angles of view of the camera (camera at a large distance from the object and/or a large zoom) this effect is practically negligible. Thirdly, which occurs only when analyzing images without distortion correction: the farther from the image center analyzed object is, the greater the elongation of the image relative to the image center is. Fourthly, applying distortion correction introduces noise to the corrected images, but this only applies to the case of images with distortion correction. All the abovementioned factors contribute to an increase in the determined bubble size. On the other hand, considering the focus set at the image center, the bubbles located outside the image center seem to be smaller, as, simply, the distance between them and camera lens is higher. This factor can contribute to a decrease in the determined bubble size, but the impact of this effect may be significant practically only at wide viewing angles.

Despite the aforementioned errors, the obtained results suggest that the benefit of conducting measurements for a larger number of frames outweighs the benefits of analyzing fewer frames where the bubble is only in the center of the image and its surroundings. In the former case, the uncertainties of determining the equivalent bubble diameters are significantly lower. Although the described influence of several factors on the increase in the values of equivalent bubble diameters seems to be apparent, the differences mostly fall within the range of measurement uncertainties.

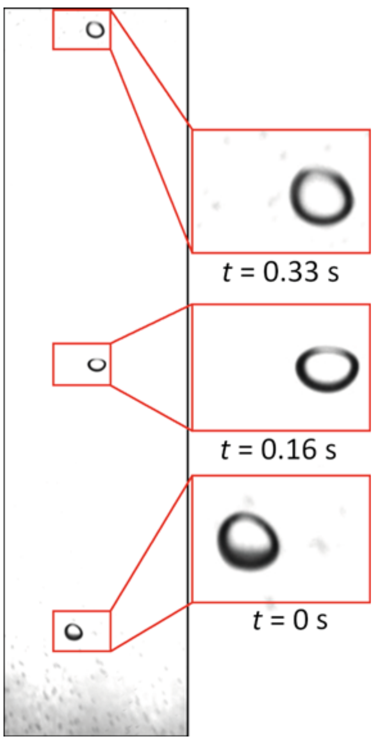

Figure 6. Example of a gas bubble during its flow, the image was created by superimposition of three video frames containing the same bubble, enlarged fragments of images are shown on the right; loss of sharpness away from the image center is visible especially when comparing upper and lower enlarged fragments to the middle enlarged fragment

Analyzing the influence of distortion correction on the obtained results and their uncertainties, it can be inferred that it leads to slightly higher values of the equivalent gas bubble diameters (Fig. 7). This suggests that the effect of increasing the diameters due to noise resulting from distortion correction dominates over the effect of eliminating the size increase caused by the distorted elongation of the image. As a result, in the experimental setup used in this work, the application of distortion correction does not seem to be justified, especially considering the lack of significant reduction in the uncertainties of determining the equivalent bubble diameters when using distortion correction. Exemplary comparison of obtained results of bubble equivalent diameters and their uncertainties determined with and without distortion correction are shown in Fig. 7.

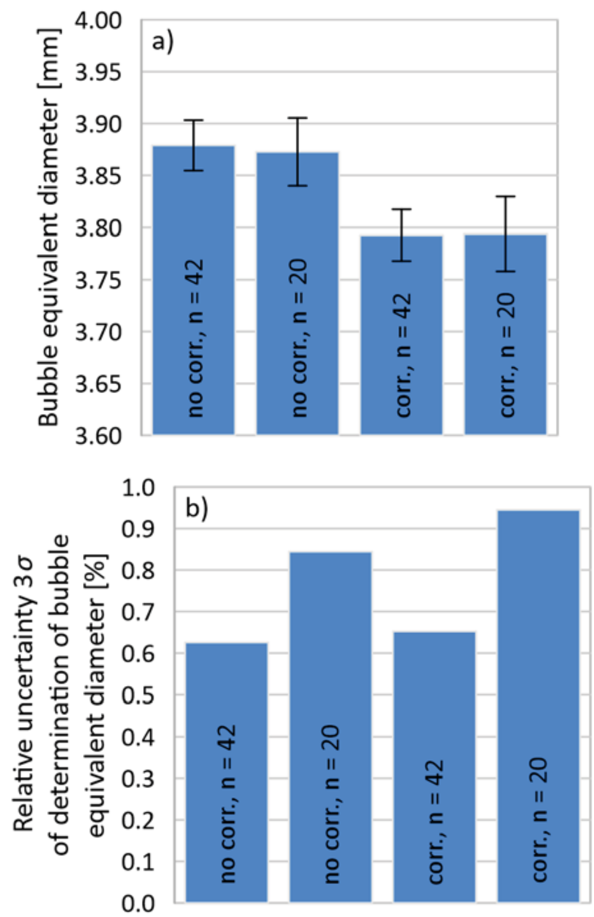

Figure 7. Bubble equivalent diameters (a) and their uncertainties (b) for cases with and without introducing image distortion correction and for different number of analyzed frames, d_i = 2.0 mm, x = 118.5 cm

In the next step, the influence of image magnification, which also determines the area covered by the camera, on the values of equivalent bubble diameters and their uncertainties was examined. The camera was set so that the distance between the averaged plane of bubble rise-up and the lens of the camera was 52.5 cm, but this time higher magnification was used (zoom increased). Optical magnification was applied, meaning that the resolution of the recorded images remained unchanged. In this part, the highest possible number of frames was analyzed for the case of higher magnification. Due to the different size of gas bubbles and changes in their apparent shape in the recorded image frames during the flow of these bubbles, in some cases the detection of the bubble in the image was unsuccessful. Sometimes the alignment of the interfacial surface caused light reflections, which made it difficult to determine the position of the interfacial boundary. Consequently, the number of analyzed frames dropped down even to 14, while the maximum number of analyzed frames was equal to 46. For lower magnification, 20 and 42 video frames were analyzed in each case, respectively. The results are presented in Fig. 8.

A significant increase in the uncertainties of determining the equivalent bubble diameters can be observed when using a higher magnification. This is mainly due to a reduction in the number of analyzed frames. Additionally, with higher magnification, the blurring effect of the bubble projection is more pronounced compared to the same bubble position in the tank but with lower camera magnification. In the case of higher magnification, the reduction in uncertainties resulting from the increased number of pixels representing the rim of the bubble in the images (projection resolution of the bubble) is much lower than the increase in uncertainty primarily caused by the reduction in the number of analyzed frames. As visible in Fig. 8, lower magnification leads to significantly lower uncertainties. The difference is not that significant for different number of analyzed frames in the case of lower magnification.

In the next stage, a comprehensive investigation of the impact of different number of analyzed frames on the obtained values of bubble equivalent diameters and their uncertainties is described. As already stated above, the profits coming from the analysis of a higher number of video frames seem to be indisputable. However, one should consider what is a reasonable minimum number of frames to be analyzed. To assess this, one recorded video showing a gas bubble significantly changing its shape during its flow was selected. The bubble was formed from the nozzle having internal diameter d_i = 1.5 mm and was recorded from the distance of x = 85.5 cm. The calculations conducted based on 79 frames led to the value of equivalent diameter equal to d_b = 3.61 ± 0.07 mm. The results of obtained bubble equivalent diameters based on single frames, as well as the final mean value with its uncertainty are shown in Fig. 9.

Next, mean values of bubble equivalent diameters and their uncertainties were calculated applying simple moving average over 5, 10, 15, 20, 25 and 30 subsequent frames. The results are shown in Fig. 10.

As can be seen, despite significantly different partial results, every value of the moving average calculated over 30 frames is within the range of the arithmetic mean value calculated using 79 frames ± its uncertainty. This leads to the conclusion that if the frame rate of 300 fps is used, the analysis of 30 frames is sufficient to satisfactorily determine the hydrodynamic parameters of the bubbles. For moving average calculated from 5 frames, the confidence intervals are sometimes lower

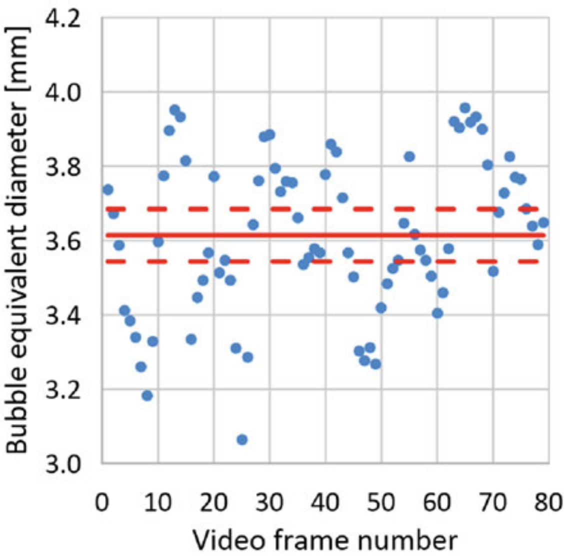

Figure 9. Bubble equivalent diameters obtained from each frame of the considered video, mean value as well as its uncertainty are indicated, respectively, using solid and dashed lines

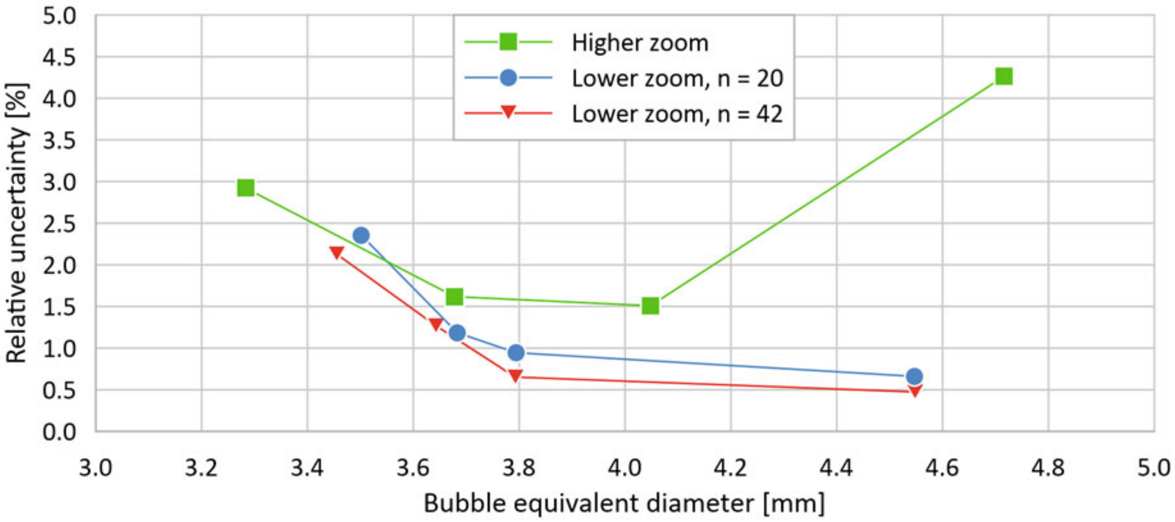

Figure 8. Relative uncertainties of calculated bubble equivalent diameters for higher and lower magnification, no distortion correction applied

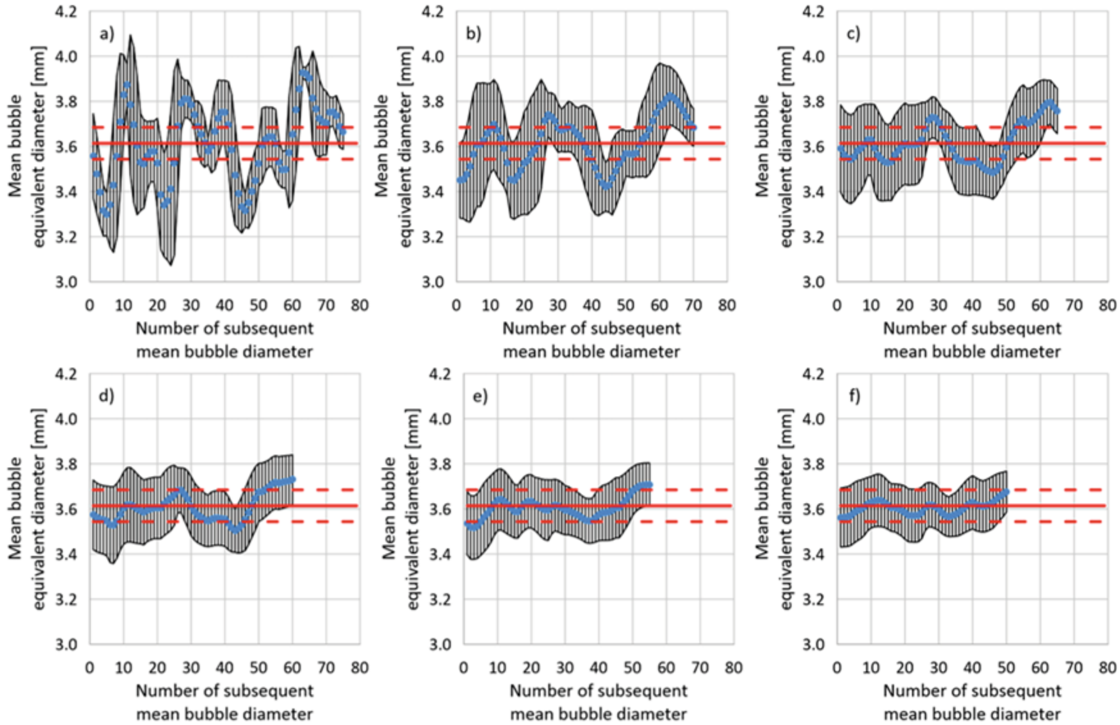

Figure 10. Mean bubble equivalent diameters obtained applying moving average over: a) 5, b) 10, c) 15, d) 20, e) 25, f) 30 subsequent frames of the considered video; arithmetic mean value from 79 frames as well as its uncertainty are indicated, respectively, using solid and dashed lines

than for the 79-frame arithmetic average, but they do not completely coincide with the value of this arithmetic average. Hence, in addition to recording at a sufficiently high frame rate, it is also crucial to record a sufficiently long fragment of the bubble flow path (sufficiently long bubble flow time).

SUMMARY AND CONCLUSIONS

The research presented in this work contributes to the precise determination of geometric parameters of gas bubbles flowing through the liquid layer, the knowledge of which is necessary for the correct determination of other quantities important from the process point of view, such as mass and heat transfer coefficients. They in turn constitute the basis for the appropriate selection of process parameters in existing equipment and in the design of new apparatuses in which liquid-gas flows are to occur.

The experimental investigation conducted within this study was focused on the examination of the influence of several factors on the determined values of the equivalent diameter of a gas bubble using the shadowgraphy method, as well as their uncertainties. These factors included: the distance between the averaged plane of bubble rise-up and the lens of the camera, the image magnification associated with the resolution of bubbles in the images, the number of analyzed frames for each bubble, and the application of image distortion correction. The obtained results suggest that the distance between the averaged plane of bubble rise-up and the camera has practically no effect on the results and their uncertainties, as long as the covered area and its resolution in the images remain constant. Increasing the number of analyzed frames significantly reduces the estimated measurement uncertainties. This is the case despite the negative impact of image blurring and distortion elongation as the bubble moves away from the image center. Increasing the image magnification, despite existence of the potential factors that could reduce uncertainties, leads to their increase because the relatively low number of analyzed frames crucially affects the increase in estimated uncertainties. Applying image distortion correction results in a minimal increase in the values of the analyzed equivalent diameters of the bubbles due to noise, while practically it has no impact on the obtained uncertainties, thus providing no justification for its application in the conditions of experiments performed within this study.

Factors such as increasing the resolution of recorded images, increasing the frame rate, and elongating the recorded flow path of the gas bubble unequivocally contribute to reducing the uncertainties in determining the equivalent bubble diameter regardless of the measurement setup. Increasing the resolution of recorded images allows the bubble to be represented by a greater number of pixels, enabling more accurate determination of its geometric parameters. Increasing the frame rate and elongating the recorded flow path of the bubble enable the analysis of a larger number of images pertaining to a specific bubble. Additionally, elongating the recorded flow path of the bubble allows capturing images of the bubble for a wider range of its changing shape during the flow, which contributes to determining the bubble equivalent diameter more accurately, especially when the bubble shape deviates significantly from a spherical shape.

The abovementioned conclusions are valid for the measurement setup used in this study. For other setups that may differ by the analyzed path of the flowing bubble or the camera and lens used, which exhibit different distortion characteristics, the results may lead to different conclusions. However, the identified sources of errors and potential possibilities for their elimination can serve as valuable guidelines for studying other multiphase systems using shadowgraphy.

Declaration of Generative AI and AI-assisted technologies in the writing process

During the preparation of this work the authors used ChatGPT 3.5 in order to improve readability and language. After using this service, the authors reviewed and edited the content as needed and take full responsibility for the content of the publication.

LITERATURE CITED

1. Besagni, G., Gallazzini, L. & Inzoli, F. (2021). Effect of gas sparger design on bubble column hydrodynamics using pure and binary liquid phases. *Chem. Eng. Sci.* 176, 116–126. DOI: 10.1016/j.ces.2017.10.036.

2. Hasan, M.N., Khan, A.A., Ahmad, S. & Lew, B. (2019). Anaerobic and aerobic sewage treatment plants in Northern India: Two years intensive evaluation and perspectives. *Environ. Technol. Innov.* 15, 100396. DOI: 10.1016/j.eti.2019.100396.

3. Luty, P. & Prończuk, M. (2020). Determination of a bubble drag coefficient during the formation of single gas bubble in upward coflowing liquid. *Processes*, 8, 8, 999. DOI: 10.3390/pr8080999.

4. Li, H. & Prakash, A. (2002). Analysis of flow patterns in bubble and slurry bubble columns based on local heat transfer measurements. *Chem. Eng. J.* 86, 3, 269–276. DOI: 10.1016/S1385-8947(01)00186-3.

5. Takayama, S. & Akita M. (2008). Bioengineering aspects of bioreactor application in plant propagation. *Plant tissue culture engineering.* (pp. 83–100). Dordrecht, Springer. DOI: 10.1007/978-1-4020-3694-1_5.

6. Xiaoping, G. & Ning, Y. (2017). Bubble properties measurement in bubble columns: From homogeneous to heterogeneous regime. *Chem. Eng. Res. Des.* 127, 103–112. DOI: 10.1016/j.cherd.2017.09.017.

7. Kulkarni, A.A. & Joshi, J.B. (2005). Bubble formation and bubble rise velocity in gas− liquid systems: a review. *Ind. Eng. Chem. Res.* 44, 16, 5873–5931. DOI: 10.1021/ie049131p.

8. Shi, S., Wang, D., Qian, Y., Sun, X., Liu, Y. & Tentner, A. (2020). Liquid-phase turbulence measurements in air-water two-phase flows using particle image velocimetry. *Prog. Nuc. Energ.* 124, 103334. DOI: 10.1016/j.pnucene.2020.103334.

9. Di Nunno, F., Granata, F., Miozzi, M., Gargano, R., de Marinis, G., Alves Pereira, F. & Di Felice, F. (2021). Experimental study of three in-line bubbles rising in still water by means of a three-dimensional (3D) shadowgraphy technique. *J. Phys. Conf. Ser.* 1977, 1, 012002. DOI: 10.1088/1742-6596/1977/1/012002.

10. Raffel, M., Willert, C.E., Scarano, F., Kähler, C.J., Wereley, S.T. & Kompenhans, J. (2018). *Particle image velocimetry: a practical guide* (3rd ed.). Springer. DOI: 10.1007/978-3-319-68852-7.

11. Di Nunno, F., Alves Pereira, F., Miozzi, M., Granata, F., Gargano, R., de Marinis, G. & Di Felice, F. (2020). Experimental study of a vertical plunging jet by means of a volumetric shadowgraph technique. *J. Phys. Conf. Ser.* 1589, 012006. DOI: 10.1088/1742-6596/1589/1/012006.

12. Zhou, X., Sun, X. & Liu, Y. (2016). Liquid-phase turbulence measurements in air-water two-phase flows over a wide range of void fractions. *Nucl. Eng. Des.* 310, 534–543. DOI: 10.1016/j.nucengdes.2016.10.048.

13. Nishino, K., Kato, H. & Torii, K. (2000). Stereo imaging for simultaneous measurement of size and velocity of particles in dispersed two-phase flow. *Meas. Sci. Technol.* 11, 6, 633–645. DOI: 10.1088/0957-0233/11/6/306.

14. Zaruba, A., Krepper, E., Prasser, H.M. & Vanga, B.R. (2005). Experimental study on bubble motion in a rectangular bubble column using high-speed video observations. *Flow Meas. Instrum.*, 16, 277–287. DOI: 10.1016/j.flowmeasinst.2005.03.009.

15. Butler, C., Cid, E. & Billet, A.-M. (2016). Modelling of mass transfer in Taylor flow: Investigation with the PLIF-I technique. *Chem. Eng. Res. Des.* 115, Part B, 292–302. DOI: 10.1016/j.cherd.2016.09.001.

16. Sathe, M.J., Thaker, I.H., Strand, T.E. & Joshi, J.B. (2010). Advanced PIV/LIF and shadowgraphy system to visualize flow structure in two-phase bubbly flows. *Chem. Eng. Sci.* 65, 8, 2431–2442. DOI: 10.1016/j.ces.2009.11.014.

17. Emberson, D.R., Ihracska, B., Imran, S. & Diez, A. (2016). Optical characterization of Diesel and water emulsion fuel injection sprays using shadowgraphy. *Fuel*, 172, 253–262. DOI: 10.1016/j.fuel.2016.01.015.

18. Nguyen, T.T., Kikura, H., Murakawa, H. & Tsuzuki, N. (2015). Measurement of Bubbly Two-phase Flow in Vertical Pipe Using Multiwave Ultrasonic Pulsed Doppler Method and Wire Mesh Tomography. *Enrgy. Proced.*, 71, 337–351. DOI: 10.1016/j.egypro.2014.11.887.

19. Rueda Villegas, L., Colombet, D., Guiraud, P., Legendre, D., Cazin, S. & Cockx, A. (2019). Image processing for the experimental investigation of dense dispersed flows: Application to bubbly flows. *Int. J. Multiphas. Flow*, 111, 16–30. DOI: 10.1016/j.ijmultiphaseflow.2018.10.017.

20. Tompkins, C., Prasser, H.M. & Corradini, M. (2018). Wire-mesh sensors: A review of methods and uncertainty in multiphase flows relative to other measurement techniques Wire-mesh sensors: A review of methods and uncertainty in multiphase flows relative to other measurement techniques. *Nucl. Eng. Des.* 337, 205–220. DOI: 10.1016/j.nucengdes.2018.06.005.

21. Murakawa, H., Shimizu, T. & Eckert, S. (2021). Development of a high-speed ultrasonic tomography system for measurements of rising bubbles in a horizontal cross-section. *Measurement*, 182, 109654. DOI: 10.1016/j.measurement.2021.109654.

22. Lucas, G.P. & Mishra, R. (2005). Measurement of bubble velocity components in a swirling gas–liquid pipe flow using a local four-sensor conductance probe. *Meas. Sci. Technol.*, 16, 749–758. DOI: 10.1088/0957-0233/16/3/018.

23. Luty, P., Prończuk, M. & Bizon, K. (2022). Experimental verification of different approaches for the determination of gas bubble equivalent diameter from optical imaging. *Chem. Eng. Res. Des.* 185, 210–222. DOI: 10.1016/j.cherd.2022.07.008.

24. Wichterle, K., Večeř, M. & Růžička, M. (2014). Asymmetric deformation of bubble shape: cause or effect of vortex-shedding?. *Chem. Pap.* 68, 1, 74–79. DOI: 10.2478/s11696-013-0406-9.

25. Canny, J. (1986). A computational approach to edge detection, *IEEE T. Pattern Anal.*, PAMI-8, 6, 679–698. DOI: 10.1109/TPAMI.1986.4767851.